Growth and characterization of InSb on (100) Si for mid-infrared application

Bo Wen Jia, Kian Hua Tan, Wan Khai Loke, Satrio Wicaksono, and Soon Fatt Yoon

School of Electrical and Electronic Engineering, Nanyang Technological University, 50 Nanyang Avenue, Singapore 639798, Republic of Singapore

Abstract

Monolithic integration of InSb on (100) Si is a practical approach to realizing on-chip mid-infrared photonic devices. An InSb layer was grown on a (100) Si substrate using an AlSb/GaSb buffer containing InSb quantum dots (QDs). The growth process for the buffer involved the growth of GaSb on Si using an interfacial misfit array, followed by InSb QDs on AlSb to decrease the density of microtwins. InSb layers were separately grown on AlSb and GaSb surfaces to compare the effect of different interfacial misfit arrays. The samples were characterized using transmission electron microscopy and x-ray diffraction to determine the structural properties of the buffer and InSb layers. The InSb on the AlSb sample exhibited higher crystal quality than the InSb on GaSb sample due to a more favorable arrangement of interfacial misfit dislocations. Hall measurements of unintentionally doped InSb layers demonstrated a higher carrier mobility in the InSb on the AlSb sample than in InSb on GaSb. Growing InSb on AlSb also improved the photoresponsivity of InSb as a photoconductor on Si.

1. Introduction

The hetero-integration of narrow bandgap semiconductors with (100) silicon substrates is a fundamental technique for the development of on-chip infrared photonic devices. These devices have a versatile range of uses, from optical communication to emerging on-chip chemical and biological sensors [1]. In particular, devices in the mid-infrared bandgap range (3–8 μm) show great application potential in on-chip optical interconnection [2], thermal imaging and sensing of specific gas molecules (NO, CO, CO_2) [3]. InSb is attracting great interest as a material for mid-infrared applications, with a cutoff

wavelength of 7.3 μm at 300 K. Heteroepitaxial growth of InSb layers on Si enables the construction of economically efficient on-chip InSb photonic devices, allowing InSb-based photonic devices and Si-based circuits to be monolithically integrated without requiring any bonding process. However, the growth of InSb on (100) Si substrates is a longstanding challenge due to the relatively high lattice mismatch (19.3%), stemming from the different lattice structures of InSb (zinc-blende) and Si (diamond-like). These differences result in a high density of defects, which suppresses device performance. Moreover, nucleation of InSb on the (100) Si surface is prohibited because Sb atoms prefer to bond with Si rather than In atoms, resulting in the formation of In metallic islands on Sb-terminated Si surfaces [4]. Therefore, a continuous InSb layer cannot be formed by direct deposition of In and Sb atoms on (100) Si, and a buffer layer between the InSb layer and the Si substrate is needed.

Mori *et al.*, attempted to grow InSb on Si through a V-grooved (100) Si substrate, found that InSb grew instead on the (111) surface [5]. To grow InSb on (100) Si, a buffer layer was needed. Materials such as Ge, AlSb and GaAs have proved to be effective buffers due to their suitable lattice constants, which are intermediate between InSb and Si [6-8]. In recent decades, a new approach to the growth of highly lattice-mismatched materials, known as the interfacial misfit (IMF) method, has been developed for cases of heteroepitaxy involving GaSb/GaAs, InSb/GaAs and AlSb/Si [9-11]. Using this method, a highly periodical IMF array consisting of pure 90° misfit dislocations is formed, which relieves most of the strain energy caused by the lattice mismatch [12], while the threading dislocations arising from the interface are minimal. Compared with 60° misfit dislocations, 90° misfit dislocations are capable of relieving higher strain energies and do not glide to form threading dislocations. This method accommodates the entire lattice mismatch at the interface without a buffer layer; however, carefully controlled growth conditions are important for the formation of the IMF array [10, 13, 14].

In this work, a new buffer structure was proposed and successfully grown using the IMF method, allowing the fabrication of an InSb photoconductor on 0° offcut (100) Si (exact (100) Si). The purpose of using 0° offcut (100) Si due to its totally compatible with

standard CMOS fabrication [15]. The formation of an IMF array significantly decreased the buffer thickness and threading dislocation density in the InSb layer. The new buffer structure included two IMF arrays. The first was located at the GaSb/Si interface. GaSb was grown on a Si substrate instead of on the more common AlSb, as AlSb on Si has been reported to have a high surface roughness [16], which can impair the subsequent growth. In addition to the threading dislocations induced by the large lattice mismatch, an anti-phase domain (APD) is the other dominant defect in InSb on a 0º offcut (100) Si. When a polar III-V semiconductor compound was grown on nonpolar Si, the formation of a monoatomic step on the Si surface caused part of the atoms of the III-V compound to be arranged in opposite order from those in an ideal lattice [17]. Most of APDs annihilate near the III-V/Si interface [18]. In some situations, the APDs result in microtwins which can propagate across the heteroepotaxial structure [19, 20]. Ko *et al.* suggested that InSb quantum dots (QDs) on an AlSb surface could act as a defect filter to suppress the microtwin associated with APD [21]. Therefore, following the growth of 120 nm GaSb and 80 nm AlSb, InSb QDs were grown on the AlSb surface. A GaSb layer was sequentially grown to cover the InSb QDs. The lattice mismatch between InSb and GaSb was accommodated through the second IMF array, which was separately formed at two interfaces-InSb/AlSb and InSb/GaSb. To investigate the effect of two different interfaces on the quality of InSb layer, two samples were grown on AlSb and GaSb as referred as “InSb on AlSb” and “InSb on GaSb” and their structural, electrical and optical properties were compared.

2. Experimental procedure

All samples were grown using a solid-state molecular beam epitaxy (MBE) system equipped with antimony (Sb) valved crackers, which provided a Sb_2 flux. The growth process was monitored by *in-situ* reflection high-energy electron diffraction (RHEED). Before growth, the Si substrates were etched with hydrofluoric acid to remove oxides on the Si surface. The substrates were transferred to the MBE chamber and heated to 950°C for 30 mins to remove residual oxides. RHEED showed a clear (2×2) pattern, which verified a pure (100) Si surface. The growth temperature was lowered to allow the growth

of GaSb. In this study, all growth was under Sb overpressure and the growth rate depended on the growth of III group elements (Al, Ga, and In).

The substrate temperature was decreased to 430°C. Two monolayers (ML) of AlSb were first grown on Si with the growth rate of 0.5 ML/s and the corresponding Sb growth rate was 0.6 ML/s. RHEED pattern changed to spotty, which indicated the formation of AlSb islands rather than a continuous AlSb layer on Si. After the deposition of AlSb, growth was interrupted for 5 mins under Sb overpressure to enhance the nucleation of AlSb islands on Si. Then, 120 nm GaSb was grown at 430°C with growth rate of 0.5 ML/s (550 nm/hr) and the corresponding Sb growth rate of 0.6 ML/s. The RHEED pattern evolved to a (3×3) pattern during the growth of GaSb.

After the growth of 120 nm GaSb, an 80 nm AlSb layer was grown at 430°C at a growth rate of 0.5 ML/s (550 nm/hr) and the corresponding Sb growth rate of 0.6 ML/s. Subsequently, InSb QDs were grown on the AlSb surface at 345°C at a growth rate of 0.62 ML/s and the corresponding Sb growth rate of 0.68 ML/s. After depositing 3 ML InSb, growth was interrupted for 30 s to enhance the surface migration of atoms to form QDs. The RHEED pattern became spotty once the growth of InSb QDs began, which indicated the formation of InSb islands on AlSb. Two different structures were grown on the QDs to optimize the material quality of the top InSb layer, as shown in Fig. 1(a). In the first structure, a 60 nm GaSb layer was grown on the QDs, followed by 40 nm AlSb. Then, the top layer of InSb was grown on the AlSb layer. In the second structure, a 100 nm GaSb layer was grown on the QDs. The top InSb layer was then grown on the GaSb layer. GaSb and AlSb were both grown at 345°C to avoid to destroy the InSb QDs, and the RHEED pattern changed to (1×3) during the growth of GaSb. The 700 nm top InSb layers were also grown at 345°C. The growth rate was 0.62 ML/s (720 nm/hr) and the corresponding Sb growth rate was 0.68 ML/s. At the initial stage of InSb growth, the RHEED patterns became spotty for about 20 s, then recovered to streaky (1×3) lines.

The structures of the samples were characterized using a scanning transmission electron microscope (STEM), as shown in Figs. 1(b) and (c), where the bottom Si substrate,

middle AlSb/GaSb buffer and top InSb are clearly shown and their thicknesses agree with the design. The poor resolution of the InSb/GaSb interface, as shown in Fig. 1(c), is due to the difference between the approximate combined atomic numbers of InSb (100) and GaSb (82). Samples were also structurally characterized using an x-ray diffractometer (XRD), high resolution TEM (HR-TEM), and near-infrared spectrophotometer. InSb photoconductors on Si were fabricated by a standard metal lift-off technique using electron beam-evaporated Au/Ti (80 nm/30 nm) to form interdigitated electrodes on the InSb surface, as shown in Fig. 1(a). The mid-infrared photoresponsivity was measured using a 700°C black body as the light source. The photoconductors were mounted on a liquid-nitrogen-cooled optical cryostat for measurement below 300 K.

3. Results and discussion

3.1 Structural properties of InSb on Si

Fig. 2(a) and (b) show [1-10]- and [110]-directional RHEED patterns, respectively, obtained during the growth of GaSb on Si when the GaSb layer thickness was about 40 nm. At both directions, [1/3]-order streaky exhibits, which is different from the reported (1×3) RHEED pattern during the GaSb grown on native substrate under Sb overpressure [22]. This (3×3) pattern can be attributed to the superposition of two (1×3) patterns from two different domains [23]. In this study, exact (100) Si substrates were used, therefore, the formation of anti-phase domain (APD) was inevitable in the GaSb layer on Si. Some APDs result in the microtwin which has distorted lattice with the surrounding lattice [19, 20]. The microtwins propagate into the surface to form different surface domains [24]. Fig. 2 (c) and (d) show a (1×3) RHEED pattern obtained the growth of GaSb above InSb QDs when the GaSb layer thickness was about 20 nm. The dispersed streak lines are due to a low growth temperature (345 °C) [25]. The disappearance of [1/3]-order streaky in the [1-10]-direction suggests the density of microtwins in the heteroepitaxial structure has been suppressed via the formation of InSb QDs on AlSb surface.

The microstructure of the GaSb/Si interface was investigated using HR-TEM as shown in Fig. 3. Fig. 3(a) shows the IMF array at the GaSb/Si interface. The bright and dark bands at the interface are attributed to bond-bending around interfacial misfit dislocations [26].

The dark bands indicate the misfit dislocations in an IMF array [27]. The separation (S) of two adjacent misfit dislocations in a highly uniform IMF array can be calculated using the following equation, assuming the lattice mismatch is completely accommodated by the IMF array [9]:

$$\mathrm{S} = \frac{b}{f} \tag{1}$$

where b is the Burgers vector of a misfit dislocation in the layer and f is the lattice mismatch between the layer and substrate. The mixture of AlSb and GaSb at the interface does not influence the calculated result due to the similar lattice constant of AlSb (6.136 Å) and GaSb (6.096 Å). The separation of misfit dislocations in Fig. 3(b) was measured to be around 3.4 nm, which agreed well with the calculated value of 3.5 nm [28, 29]. Fig. 3(b) shows the upper region of GaSb layer on Si where two microtwins propagating from the interface are indicated. Their orientations are opposite and both microtwins have inclination angles of 54.7° with the Si substrate. Some 90° interfacial misfit dislocations locate at the GaSb/Si interface. At the bottom of the left microtwin, a trigonal-shaped defect is observed. In the zinc-blend structure, the boundary of APD easily forms along {111} lattice planes. Two boundaries with opposite orientations may annihilate during the growth and form a trigonal-shaped defect [30]. The coincident distribution of APD and microtwin implies the APD generates microtwin which has been suggested by previous reports [19, 20]. The detailed structure of a microtwin is shown in Fig. 3(c) where the (1-11) lattice planes in the normal GaSb lattices are marked by white lines and the (1-11) lattice plane in the microtwin is marked by red line. Two twin boundaries are marked by dashed lines. The microtwin propagates along the (-111) lattice plane. The (1-11) lattice plane in the microtwin tilts by 37.5º with the two neighbored (1-11) lattices in the normal GaSb and the width of the microtwin is about 1 nm. The microtwin can be suppress through InSb QDs on AlSb which will be presented in Fig. 5.

Figs. 4(a) and (b) show the x-ray (115) reciprocal space maps (RSMs) of InSb on AlSb and on GaSb surfaces, respectively. Diagonal dashed lines indicate the fully relaxed reciprocal lattice peaks. In both samples, four peaks, representing (from top to bottom) the Si, GaSb, AlSb and InSb layers, were found in each RSM. Using the reciprocal lattice

vectors Q_X and Q_Z of the InSb peak in the RSM, the vertical ($a_\perp$) and parallel ($a_{//}$) lattice constants of the InSb layer were calculated. The calculated results are listed in Table I. The InSb layers in both samples were nearly 100% relaxed. The positions of both the GaSb and AlSb peaks deviated from the dashed line. These two peaks were in fact aligned along a vertical line, which was parallel to the Q_z axis. From this line, both peaks were calculated to have an identical $a_{\parallel}$ of about 6.117 Å. Note also that the AlSb peak deviated to the right of the dashed line, while the GaSb peak deviated to the left. The AlSb layer was compressively strained, while GaSb was slightly tensile-strained. The only observable difference between Figs. 4(a) and (b) is the intensity of the AlSb peaks: the peak in Fig. 4 (a) is higher, due to the different thickness of the AlSb layers in the two samples.

Table 1

Lattice constants, relaxation, FWHM from (004) ω scan, 300 K carrier mobility and concentration of InSb on AlSb and InSb on GaSb

Structure	$a_\perp$ (Å)	$a_{//}$ (Å)	Relaxation (%)	(004) ω scan FWHM (arcsec.)	300 K carrier mobility (cm^2/Vs)	300 K carrier concentration (cm^{-3})
InSb on AlSb	6.491	6.474	99.5	810.8	20202	3.76×10^{16}
InSb on GaSb	6.499	6.471	99.2	904.0	17700	4.25×10^{16}

The effectiveness of the InSb QDs in defect filtering was assessed using cross-section TEM (Figs. 5(a)-(f)). Figs. 5(a)-(c) show low-magnification TEM images of InSb on AlSb, where (a) shows the entire AlSb/GaSb buffer structure, including the top layer of AlSb, (b) shows the InSb layer grown on AlSb, with no obvious dislocations arising from the InSb/AlSb interface, (c) shows the InSb layer grown on GaSb, with some defects arising from the interface. In Fig. 5(a), a high density of defects arising from the GaSb/Si interface can be seen. These defects propagated through the first GaSb and AlSb layers. InSb QDs with diameters of ~20 nm and heights of ~10 nm were observed at the surface

of the first AlSb layer. The distribution of InSb QDs was irregular because of their preference to nucleate at defect sites. A detailed visualization of the InSb QDs is presented in Fig. 5(d), where a defect with a different crystal structure from the surrounding material is terminated by an InSb QD. Fast Fourier transformation of the TEM image was carried out in area E, located above an InSb QD, and area F, containing defects. The diffraction patterns for each area are shown in Figs. 5(e) and (f). Both areas present standard diffraction patterns of the zinc blende structure. However, in Fig. 5(f), extra diffraction points with weak intensity are observed between the peaks of the standard pattern. It is known that microtwins can tilt the crystal orientation to a certain degree with respect to the orientation of the surrounding material. This tilt introduces extra diffraction points, which serve as a clear indicator of the presence of microtwins [31]. As the microtwins here have different crystal orientations from the rest of the AlSb layer, they result in steps at the AlSb surface. Previous research suggested that microtwins could be terminated by the preferential nucleation of InSb QDs on AlSb at these steps [21]. In Fig. 5(a), the GaSb layer above the InSb QDs is nearly defect-free due to the defect-filtering function of the InSb QDs.

Two InSb layers were grown on the AlSb and GaSb surfaces, respectively, as mentioned earlier. The InSb/AlSb interface is shown in the upper part of Fig. 5(a) and the lower part of Fig. 5(b), both of which show a high density of defects at the interface. When samples are grown using IMF arrays, a high density of misfit dislocations is generally formed at the interface. If all of the misfit dislocations are oriented at 90° and their separation is uniform, the strain induced by the lattice mismatch can be entirely accommodated by the IMF array [12, 32]. Threading dislocations originate from a non-uniform IMF array and the presence of 60° misfit dislocations [33]. As listed in Table I, the FWHM in the (004) ω-scan of InSb on AlSb is narrower than that of InSb on GaSb. Therefore, the density of threading dislocations is lower in the InSb on AlSb sample, as the presence of threading dislocations broadens the (004) ω-scan FWHM [34]. Moreover, Fig. 5(c) shows some dislocations arises from the InSb/GaSb interface, while, no dislocation is observed in Fig. 5(b), which supports the result of ω-scan. Figs. 6(a)-(d) compare the interfacial dislocations at the InSb/AlSb and InSb/GaSb interfaces in detail.

Cross-sectional TEM images of the InSb/AlSb and InSb/GaSb interfaces are respectively shown in Figs. 6(a) and (c). Although black interfaces can be observed in both images, no further structural information can be obtained by visual inspection. To enable a meaningful analysis of the misfit dislocations at the interfaces, a Fourier mask filtering technique was applied to Figs. 6(a) and (c) to obtain the atomic arrangements at the interfaces shown in Figs. 6(b) and (d), respectively. A 90° misfit dislocation is associated with two extra planes, while a 60° misfit dislocation is associated with one extra plane. The extra planes in Figs. 6(b) and (d) are indicated by arrows. Fig. 6(b) exhibits uniformly distributed 90° misfit dislocations at the InSb/AlSb interface. In contrast, one 60° misfit dislocation and three at 90° are observed at the InSb/GaSb interface. The 60° misfit dislocations can glide on the (111) lattice planes to form threading dislocations, leading to the wider (004) ω-scan FWHM of InSb on GaSb compared with that of InSb on AlSb.

Some mechanisms were proposed to explain the selectivity of forming 60° or 90° misfit dislocation in the lattice-mismatched heteroepitaxy, such as different lattice mismatch [35], the offcut of substrate [36] and growth mode. In this study, the lattice mismatch between InSb/AlSb and InSb/GaSb were approximate and all substrates were exact (100) Si. As mentioned in the experimental procedure, the RHEED patterns became spotty for about 20 s, then recovered to streaky (1×3) lines at the initial growth of InSb layer on GaSb or AlSb. Therefore, the growth mode of InSb layer in this study should be to Volmer-Weber (island-like) or Stranski-Krastanow [37]. The InSb islands directly form on AlSb or GaSb in the Volmer-Weber mode. The Stranski-Krastanow growth mode starts with the growth of a two-dimensional strained layer and switches to that of a relaxed island after exceeding a critical thickness. The islands coalesce into a continuous layer during the subsequent growth. Compared with the Stranski-Krastanow mode, the Volmer-Weber mode requires a lager lattice mismatch or a larger difference in the surface energy [38]. Both experimental and theoretical investigations of IMF array suggested pure 90° misfit dislocations form at the interface between layer and substrate through periodic skipping of chemical bonds [9, 32], which agrees with the Volmer-Weber growth mode. The surface energy of InSb is known to be 17.3% lower than that of AlSb and 5.8% lower

than that of GaSb [39]. This suggests that the growth mode of InSb on GaSb may be different from that of InSb on AlSb. Previous studies of InSb QDs grown on GaSb indicated that the growth of InSb on GaSb occurred via the Stranski-Krastanow mode [40, 41]. Under the Stranski-Krastanow mode, misfit dislocations mainly form at the interface between the edge of the island and the strained layer [35, 42]. The possibility of forming 60º misfit dislocations is higher at the edge of the island due to a high shear stress [43].

3.2 Electrical properties of InSb on Si

The carrier mobility in a semiconductor depends on the density of threading dislocations within it, and is therefore considered a criterion to evaluate the quality of the layer. Moreover, in a photoconductor, high carrier mobility results in high gain [44]. In this study, the InSb layers on both AlSb and GaSb were unintentionally n-type doped. Figs. 7(a) and (b) show the temperature-dependent carrier mobility and concentration of InSb layers; the electron mobilities at 300 K are also listed in Table I. The temperature-dependent intrinsic electron concentration (n_i) in bulk InSb above 200 K can be described using the following equation [45]:

$$n_i = 5.76 \times 10^{14} T^{1.5} \exp\left(-\frac{0.129}{k_B T}\right) \quad (2)$$

where k_B is the Boltzmann constant and T is the temperature. The temperature dependence of the mobility and concentration differ from those of other semiconductors, where mobility decreases while concentration increases with the increasing temperature, and this difference is attributed to the dislocations near the interface (of both misfit and threading type) [10, 46, 47]. The concentrations measured above 200 K are clearly higher than the calculated n_i, indicating that extrinsic electrons participate in current transport in the InSb layer. The extrinsic electrons originate from dislocations near the InSb/AlSb and InSb/GaSb interfaces [48], and result in the formation of impurity bands in the region near the interface due to the small effective mass of the electrons and the large Bohr radius of the donor in InSb [49]. The impurity bands are located below the Fermi level of InSb, which is characteristic of degenerated semiconductors [50]; therefore, the InSb layer on Si in this study may be a heterostructure, in which the region near the interface has the properties of a degenerated semiconductor while the bulk region has those of a

normal semiconductor. The inhomogeneity of the InSb layer on Si results in the complicated temperature-dependent mobility and concentration, especially at a low temperature, a detailed explanation of which can be found elsewhere [47]. At 300 K, the mobility of InSb on AlSb is higher than that of InSb on GaSb. As mentioned previously, the 60° misfit dislocations forming at the interface can glide to form threading dislocations, which act as defect-related scattering centers to suppress the mobility of carriers [51]. As the growth conditions for both InSb layers are the same, the higher mobility in InSb on AlSb indicates a lower threading dislocation density, which is consistent with the previous XRD and TEM results.

3.3 InSb photoconductor on Si

The photocurrents of the InSb photoconductors were measured under a black body maintained at 700°C as a function of DC applied voltage, as shown in Figs. 8(a) and (b). An optical microscopic image of a photoconductor is shown in the inset of Fig. 8(b), where the separation of two adjacent electrodes is about 13.3 μm. The photocurrent increased linearly with the increasing voltage at both 77 and 140 K, a feature of photoconductive gain. The gain (G) can be expressed as [44]

$$\mathrm{G} = \tau\left(\frac{1}{t_e} + \frac{1}{t_h}\right) \tag{3}$$

where τ is the minority carrier lifetime and t_e and t_h are the transit times of electrons and holes, respectively. Therefore, a high carrier lifetime and a low transit time both contribute to an increase in responsivity (or photoconductive gain). The transit time (t) for holes or electrons can be calculated using [44]

$$t = \frac{L^2}{\mu V} \tag{4}$$

where L is the separation of electrodes, μ is the mobility of electrons or holes and V is the applied voltage. Higher voltages result in shorter transit times, leading to higher responsivity. The insets in Figs. 8(a) and (b) show the temperature-dependent photocurrent for the InSb photoconductors on AlSb and GaSb, respectively. The photocurrent was observed to decrease with increasing temperature. At temperatures below 150 K, the decrease in minority carrier lifetime and increase in thermal generation

of carriers suppressed the responsivity [52]. The InSb photoconductor on AlSb demonstrated a higher responsivity than that on GaSb under all measurement conditions (applied voltage and temperature). This observation is consistent with the higher threading dislocation density in the InSb on GaSb sample discussed earlier. Threading dislocations can act as recombination centers, resulting in a low minority carrier lifetime [53]. Therefore, further suppressing the density of threading dislocations is necessary to improve the performance of InSb photoconductors on Si.

4. Conclusions

In conclusion, we demonstrated the growth of InSb through an AlSb/GaSb buffer on (100) Si substrates. A GaSb layer of thickness 120 nm was first grown on Si at 430°C, with an AlSb prelayer to accommodate the lattice mismatch between GaSb and Si. AlSb with a thickness of 80 nm was subsequently grown, and InSb QDs were finally grown on the AlSb surface to suppress microtwins, the success of which was confirmed using TEM. For the top layer of the buffer, two structures were compared. The first was 100 nm GaSb, which provided a GaSb surface for the growth of InSb. The other comprised 60 nm GaSb topped with 40 nm AlSb to provide an AlSb surface. XRD, TEM and Hall measurements indicated that the InSb layer on AlSb had a narrower FWHM of ω-scanning, a more uniform interfacial misfit array and higher mobility. The InSb photoconductors were demonstrated to operate even below 150 K, while the InSb photodetector on AlSb showed higher responsivity than that on GaSb. The buffer structure and growth conditions proposed in this work could provide an approach to integrating InSb-based devices on Si.

Acknowledgements

This work was supported by Singapore National Research Foundation through the Competitive Research Program (Grant No: NRF-CRP6-2010-4). The authors of this paper would like to express their gratitude to Dr. Tong Jinchao and Mr. Zheng Yi for their assistance with the photoconductor measurement and valuable discussion.

References:

[1] V. Singh, P.T. Lin, N. Patel, H. Lin, L. Li, Y. Zou, F. Deng, C. Ni, J. Hu, J. Giammarco, Mid-infrared materials and devices on a Si platform for optical sensing, Sci. Technol. Adv. Mater. , 15 (2014) 014603.

[2] R. Soref, Mid-infrared photonics in silicon and germanium, Nat. Photonics 4(2010) 495-497.

[3] M. Razeghi, Overview of antimonide based III-V semiconductor epitaxial layers and their applications at the center for quantum devices, Eur Phys J-Appl Phys, 23 (2003) 149-205.

[4] G. Franklin, D. Rich, H. Hong, T. Miller, T.-C. Chiang, Interface formation and growth of InSb on Si (100), Phys. Rev. B, 45 (1992) 3426.

[5] M. Mori, S. Khamseh, T. Iwasugi, K. Nakatani, K. Murata, M. Saito, K. Maezawa, InSb films grown on the V-grooved Si (001) substrate with InSb bilayer, Physics Procedia, 3 (2010) 1335-1339.

[6] E. Michel, J. Xu, J. Kim, I. Ferguson, M. Razeghi, InSb infrared photodetectors on Si substrates grown by molecular beam epitaxy, IEEE Photonics Technol. Lett. , 8 (1996) 673-675.

[7] M. Mori, N. Akae, K. Uotani, N. Fujimoto, T. Tambo, C. Tatsuyama, Heteroepitaxial growth of InSb films on a Si (0 0 1) substrate via AlSb buffer layer, Appl. Surf. Sci. , 216 (2003) 569-574.

[8] M. Mori, Y. Tsubosaki, T. Tambo, H. Ueba, C. Tatsuyama, Growth of InSb films on a Si (001) substrate with Ge buffer layer, Appl. Surf. Sci. , 117 (1997) 512-517.

[9] S.H. Huang, G. Balakrishnan, A. Khoshakhlagh, A. Jallipalli, L.R. Dawson, D.L. Huffaker, Strain relief by periodic misfit arrays for low defect density GaSb on GaAs, Appl. Phys. Lett. , 88 (2006).

[10] B.W. Jia, K.H. Tan, W.K. Loke, S. Wicaksono, S.F. Yoon, Formation of periodic interfacial misfit dislocation array at the InSb/GaAs interface via surface anion exchange, J. Appl. Phys. , 120 (2016) 035301.

[11] J. Tatebayashi, A. Jallipalli, M.N. Kutty, S. Huang, K. Nunna, G. Balakrishnan, L.R. Dawson, D.L. Huffaker, Monolithically integrated III-Sb-based laser diodes grown on miscut Si substrates, IEEE J. Sel. Top. Quantum Electron. , 15 (2009) 716-723.

[12] A. Trampert, E. Tournie, K. Ploog, Novel plastic strain-relaxation mode in highly mismatched III-V layers induced by two-dimensional epitaxial growth, Appl. Phys. Lett. , 66 (1995) 2265-2267.

[13] K.H. Tan, B.W. Jia, W.K. Loke, S. Wicaksono, S.F. Yoon, Formation of interfacial misfit dislocation in GaSb/GaAs heteroepitaxy via anion exchange process, J. Cryst. Growth 427 (2015) 80-86.

[14] B.W. Jia, K.H. Tan, W.K. Loke, S. Wicaksono, S.F. Yoon, Effects of surface reconstruction on the epitaxial growth of III-Sb on GaAs using interfacial misfit array, Appl. Surf. Sci. , (2016).

[15] K. Volz, A. Beyer, W. Witte, J. Ohlmann, I. Németh, B. Kunert, W. Stolz, GaP-nucleation on exact Si (001) substrates for III/V device integration, J. Cryst. Growth 315 (2011) 37-47.

[16] G. Balakrishnan, S. Huang, L. Dawson, Y.-C. Xin, P. Conlin, D. Huffaker, Growth mechanisms of highly mismatched AlSb on a Si substrate, Appl. Phys. Lett. , 86 (2005) 034105.

[17] I. Németh, B. Kunert, W. Stolz, K. Volz, Heteroepitaxy of GaP on Si: Correlation of morphology, anti-phase-domain structure and MOVPE growth conditions, J. Cryst. Growth 310 (2008) 1595-1601.
[18] O. Skibitzki, F. Hatami, Y. Yamamoto, P. Zaumseil, A. Trampert, M. Schubert, B. Tillack, W. Masselink, T. Schroeder, GaP collector development for SiGe heterojunction bipolar transistor performance increase: A heterostructure growth study, J. Appl. Phys. , 111 (2012) 073515.
[19] G. Devenyi, S. Woo, S. Ghanad-Tavakoli, R. Hughes, R. Kleiman, G. Botton, J. Preston, The role of vicinal silicon surfaces in the formation of epitaxial twins during the growth of III-V thin films, J. Appl. Phys. , 110 (2011) 124316.
[20] V. Narayanan, S. Mahajan, K. Bachmann, V. Woods, N. Dietz, Antiphase boundaries in GaP layers grown on (001) Si by chemical beam epitaxy, Acta Mater. , 50 (2002) 1275-1287.
[21] K.-M. Ko, J.-H. Seo, D.-E. Kim, S.-T. Lee, Y.-K. Noh, M.-D. Kim, J.-E. Oh, The growth of a low defect InAs HEMT structure on Si by using an AlGaSb buffer layer containing InSb quantum dots for dislocation termination, Nanotechnology, 20 (2009) 225201.
[22] M. Sieger, T. Miller, T.-C. Chiang, Reflection high-energy electron diffraction and photoemission study of GaSb (100) reconstructions, Phys. Rev. B, 52 (1995) 8256.
[23] M. Debnath, T. Mishima, M. Santos, K. Hossain, O. Holland, Improved electron mobility in InSb epilayers and quantum wells on off-axis Ge (001) substrates, J. Appl. Phys. , 111 (2012) 073525.
[24] K. Aït-Mansour, D. Dentel, L. Kubler, M. Diani, J. Bischoff, D. Bolmont, Epitaxy relationships between Ge-islands and SiC (0001), Appl. Surf. Sci. , 241 (2005) 403-411.
[25] T. Chiu, W. Tsang, Reflection high-energy electron diffraction studies on the molecular-beam-epitaxial growth of AISb, GaSb, InAs, InAsSb, and GaInAsSb on GaSb, J. Appl. Phys. , 57 (1985) 4572-4577.
[26] M. De Giorgi, A. Taurino, A. Passaseo, M. Catalano, R. Cingolani, Interpretation of phase and strain contrast of TEM images of In x Ga 1− x A s/G a A s quantum dots, Phys. Rev. B, 63 (2001) 245302.
[27] S.H. Huang, G. Balakrishnan, A. Khoshakhlagh, L.R. Dawson, D.L. Huffaker, Simultaneous interfacial misfit array formation and antiphase domain suppression on miscut silicon substrate, Appl. Phys. Lett. , 93 (2008).
[28] S.H. Vajargah, S. Ghanad-Tavakoli, J. Preston, R. Kleiman, G. Botton, Growth mechanisms of GaSb heteroepitaxial films on Si with an AlSb buffer layer, J. Appl. Phys. , 114 (2013) 113101.
[29] J. Rodriguez, K. Madiomanana, L. Cerutti, A. Castellano, E. Tournié, X-ray diffraction study of GaSb grown by molecular beam epitaxy on silicon substrates, J. Cryst. Growth 439 (2016) 33-39.
[30] M. Kawabe, T. Ueda, Self-annihilation of antiphase boundary in GaAs on Si (100) grown by molecular beam epitaxy, Jpn J Appl Phys, 26 (1987) L944.
[31] T. Mishima, J. Keay, N. Goel, M. Ball, S. Chung, M. Johnson, M. Santos, Effect of micro-twin defects on InSb quantum wells, Journal of Vacuum Science & Technology B: Microelectronics and Nanometer Structures Processing, Measurement, and Phenomena, 23 (2005) 1171-1173.
[32] A. Jallipalli, G. Balakrishnan, S.H. Huang, A. Khoshakhlagh, L.R. Dawson, D.L.

Huffaker, Atomistic modeling of strain distribution in self-assembled interfacial misfit dislocation (IMF) arrays in highly mismatched III-V semiconductor materials, J. Cryst. Growth 303 (2007) 449-455.
[33] Y. Wang, P. Ruterana, S. Kret, S. El Kazzi, L. Desplanque, X. Wallart, The source of the threading dislocation in GaSb/GaAs hetero-structures and their propagation mechanism, Appl. Phys. Lett. , 102 (2013).
[34] B. Heying, X. Wu, S. Keller, Y. Li, D. Kapolnek, B. Keller, S.P. DenBaars, J. Speck, Role of threading dislocation structure on the x-ray diffraction peak widths in epitaxial GaN films, Appl. Phys. Lett. , 68 (1996) 643-645.
[35] Y. Chen, X. Lin, Z. Liliental-Weber, J. Washburn, J. Klem, J. Tsao, Dislocation formation mechanism in strained $In_xGa_{1-x}As$ islands grown on GaAs (001) substrates, Appl. Phys. Lett. , 68 (1996) 111-113.
[36] Y.B. Bolkhovityanov, A. Deryabin, A. Gutakovskii, L. Sokolov, Features of formation and propagation of 60° and 90° misfit dislocations in Ge_xSi_{1-x}/Si (x∼ 0.4-0.5) films caused by Si substrate misorientation from (001), Appl. Phys. Lett. , 92 (2008) 131901.
[37] M. Copel, M. Reuter, E. Kaxiras, R. Tromp, Surfactants in epitaxial growth, Phys. Rev. Lett. , 63 (1989) 632.
[38] K. Nakajima, Equilibrium Phase Diagrams for Stranski-Krastanov Structure Mode of III–V Ternary Quantum Dots, Jpn J Appl Phys, 38 (1999) 1875.
[39] W. Liu, W. Zheng, Q. Jiang, First-principles study of the surface energy and work function of III-V semiconductor compounds, Phys. Rev. B, 75 (2007) 235322.
[40] X. Weng, N.G. Rudawski, P.T. Wang, R.S. Goldman, D.L. Partin, J. Heremans, Effects of buffer layers on the structural and electronic properties of InSb films, J. Appl. Phys. , 97 (2005).
[41] J. Bomphrey, M. Ashwin, T. Jones, The formation of high number density InSb quantum dots, resulting from direct InSb/GaSb (001) heteroepitaxy, J. Cryst. Growth 420 (2015) 1-5.
[42] Y. Chen, J. Washburn, Structural transition in large-lattice-mismatch heteroepitaxy, Phys. Rev. Lett. , 77 (1996) 4046.
[43] H. Tsai, R. Matyi, Generation of misfit dislocations in GaAs grown on Si, Appl. Phys. Lett. , 55 (1989) 265-267.
[44] S.M. Sze, K.K. Ng, Physics of semiconductor devices, John wiley & sons, 2006.
[45] R. Cunningham, J. Gruber, Intrinsic Concentration and Heavy-Hole Mass in InSb, J. Appl. Phys. , 41 (1970) 1804-1809.
[46] J.J. Harris, T. Zhang, W.R. Branford, S.K. Clowes, M. Debnath, A. Bennett, C. Roberts, L.F. Cohen, The role of impurity band conduction in the low temperature characteristics of thin InSb films grown by molecular beam epitaxy, Semicond. Sci. Technol. , 19 (2004) 1406-1410.
[47] B.W. Jia, K.H. Tan, W.K. Loke, S. Wicaksono, S.F. Yoon, Effects of surface reconstruction on the epitaxial growth of III-Sb on GaAs using interfacial misfit array, Appl. Surf. Sci. , 399 (2017) 220-228.
[48] Y.A. Osipyan, Y.I. Fedyaev, Donor Action of Dislocations in Insb, Jetp Lett-Ussr, 9 (1969) 21-&.
[49] F. Stern, R.M. Talley, Impurity Band in Semiconductors with Small Effective Mass, Phys. Rev., 100 (1955) 1638-1643.

[50] J. Harris, T. Zhang, W. Branford, S. Clowes, M. Debnath, A. Bennett, C. Roberts, L. Cohen, The role of impurity band conduction in the low temperature characteristics of thin InSb films grown by molecular beam epitaxy, Semicond. Sci. Technol. , 19 (2004) 1406.
[51] M. Oszwaldowski, Scattering of Electrons by Charged Dislocations in Insb-Type Semiconductors, J. Phys. Chem. Solids 46 (1985) 791-796.
[52] B.R. Conley, J. Margetis, W. Du, H. Tran, A. Mosleh, S.A. Ghetmiri, J. Tolle, G. Sun, R. Soref, B. Li, Si based GeSn photoconductors with a 1.63 A/W peak responsivity and a 2.4 μ m long-wavelength cutoff, Appl. Phys. Lett. , 105 (2014) 221117.
[53] S. Shin, J. Arias, M. Zandian, J. Pasko, R. DeWames, Effect of the dislocation density on minority-carrier lifetime in molecular beam epitaxial HgCdTe, Appl. Phys. Lett. , 59 (1991) 2718-2720.

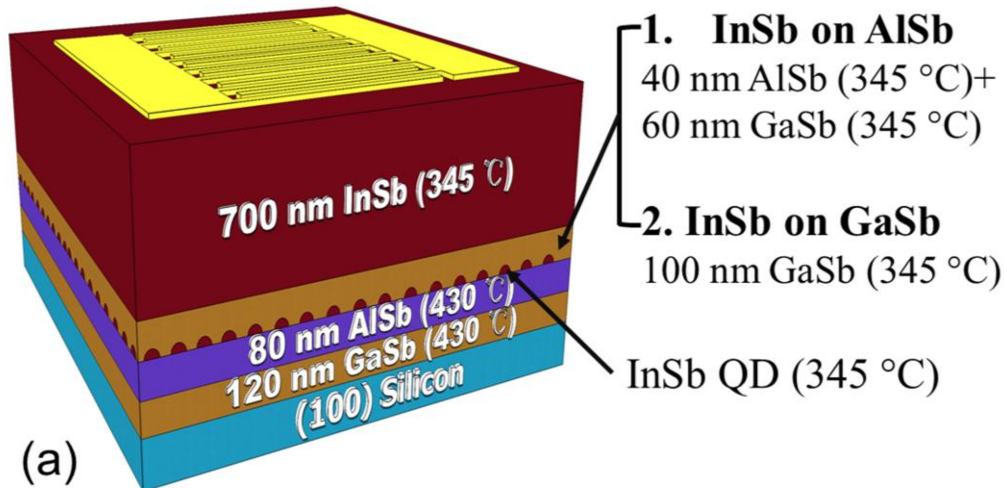

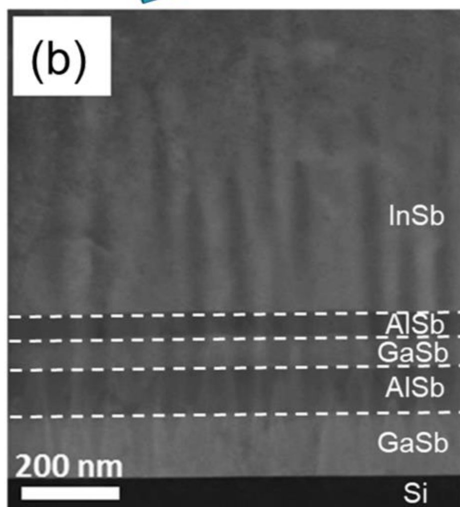

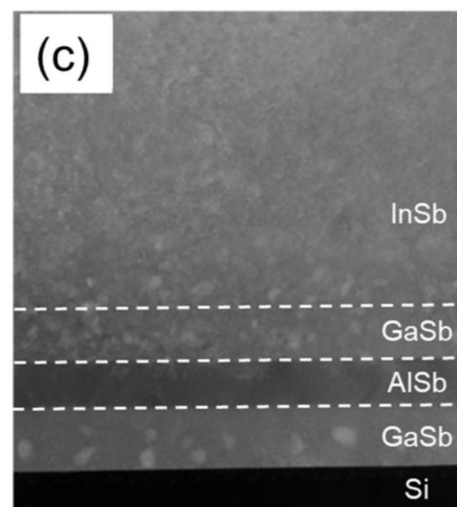

Fig.1 (a) Schematic of InSb-based photoconductors grown on (100) Si substrates. The growth temperatures of layers were indicated. (b) STEM image of InSb on AlSb buffer. (c) STEM image of InSb on GaSb buffer.

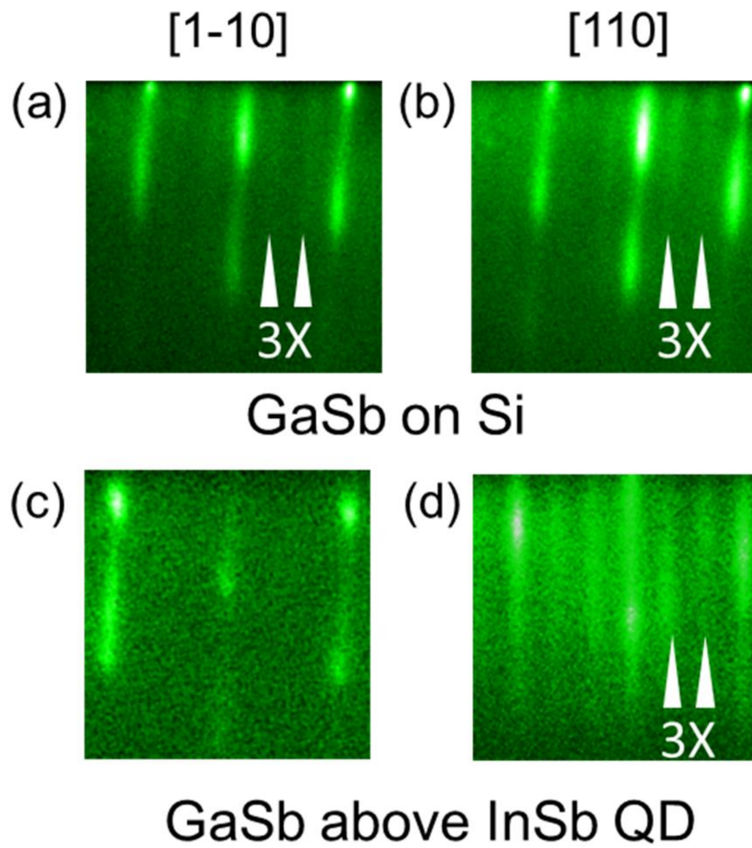

Fig. 2 [1-10]- and [110]- directional RHEED patterns during the growth of GaSb. (a) and (b) The GaSb layer grown on Si. (c) and (d) The GaSb layer grown above InSb quantum dots (QDs). The positions of fractional order streaks are indicated by white triangle.

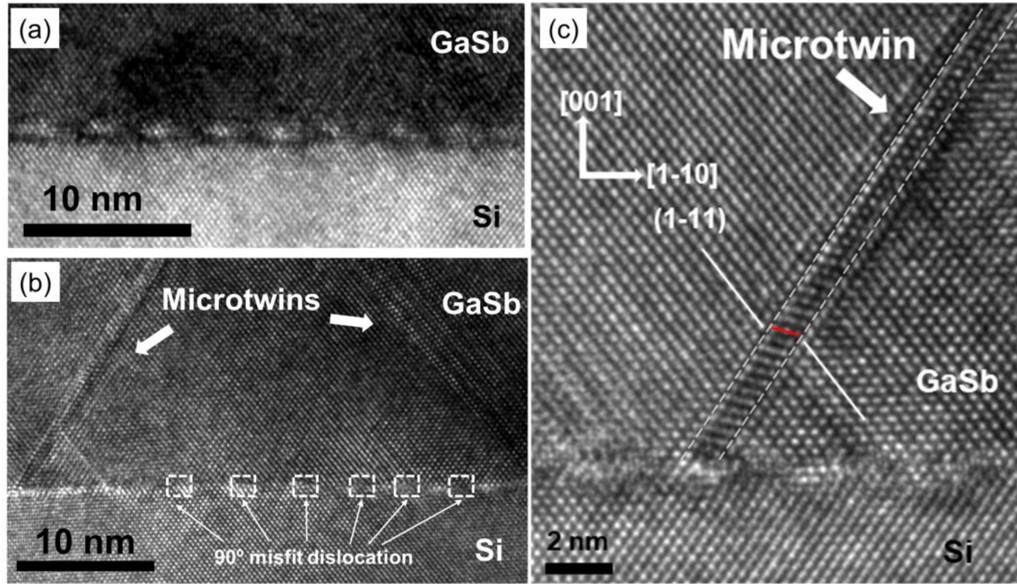

Fig. 3 High resolution TEM images of (a) the IMF array at the GaSb/Si interface; (b) microtwins in the GaSb layer on Si, where the microtwins and misfit dislocations are indicated by white arrows, respectively; (c) the detailed structure of a microtwin in the GaSb layer. Two (1-11) lattice planes in the normal GaSb lattice are indicated by white lines and one (1-11) lattice plane in the microtwin is indicated by a red line. The microtwin boundaries are indicated by dashed lines.

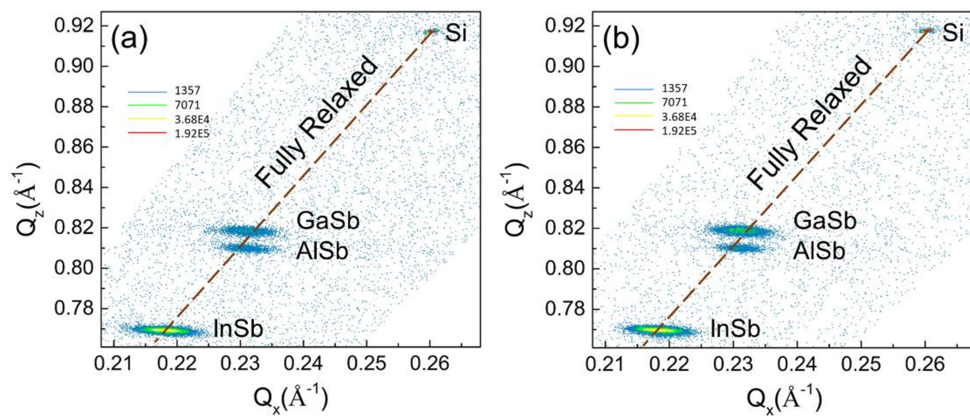

Fig. 4 X-ray (115) reciprocal space maps of (a) InSb grown on AlSb surface; (b) InSb grown on GaSb surface.

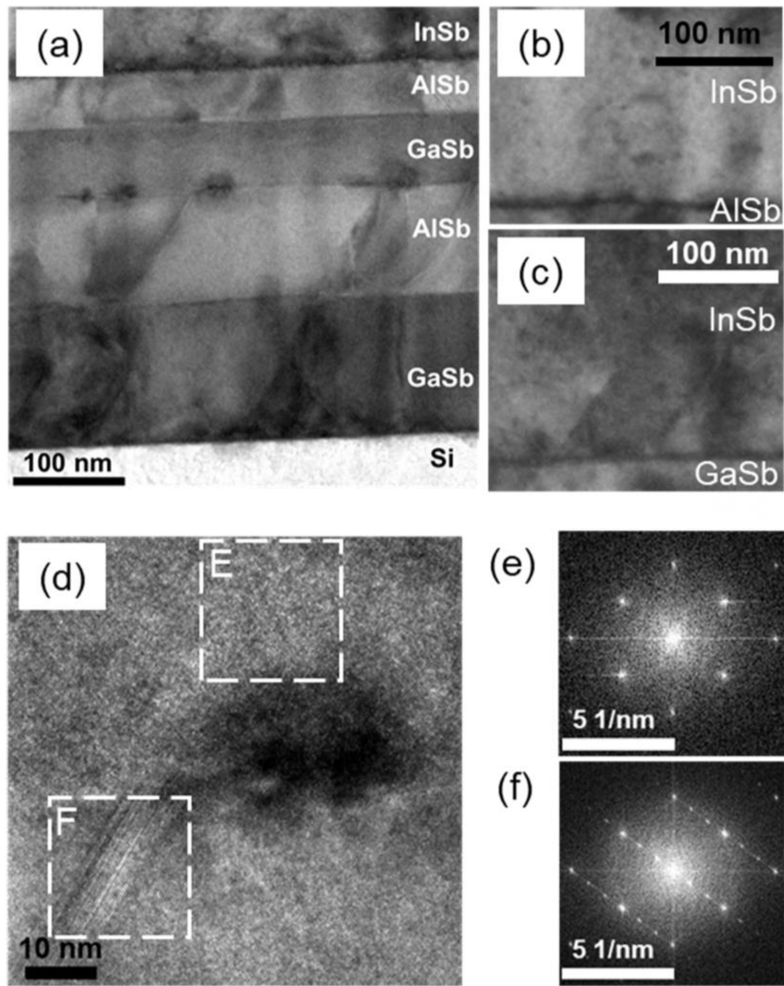

Fig. 5(a)-(c) Bright-field TEM images of InSb grown on (100) Si: (a) the AlSb/GaSb buffer containing InSb QDs; (b) InSb grown on AlSb; (c) InSb grown on GaSb. (d) High resolution TEM images of an InSb QD at the GaSb/AlSb interface. (e) and (f) diffraction patterns obtained using fast Fourier transform (FFT) in the area E and F which are indicated by white boxes.

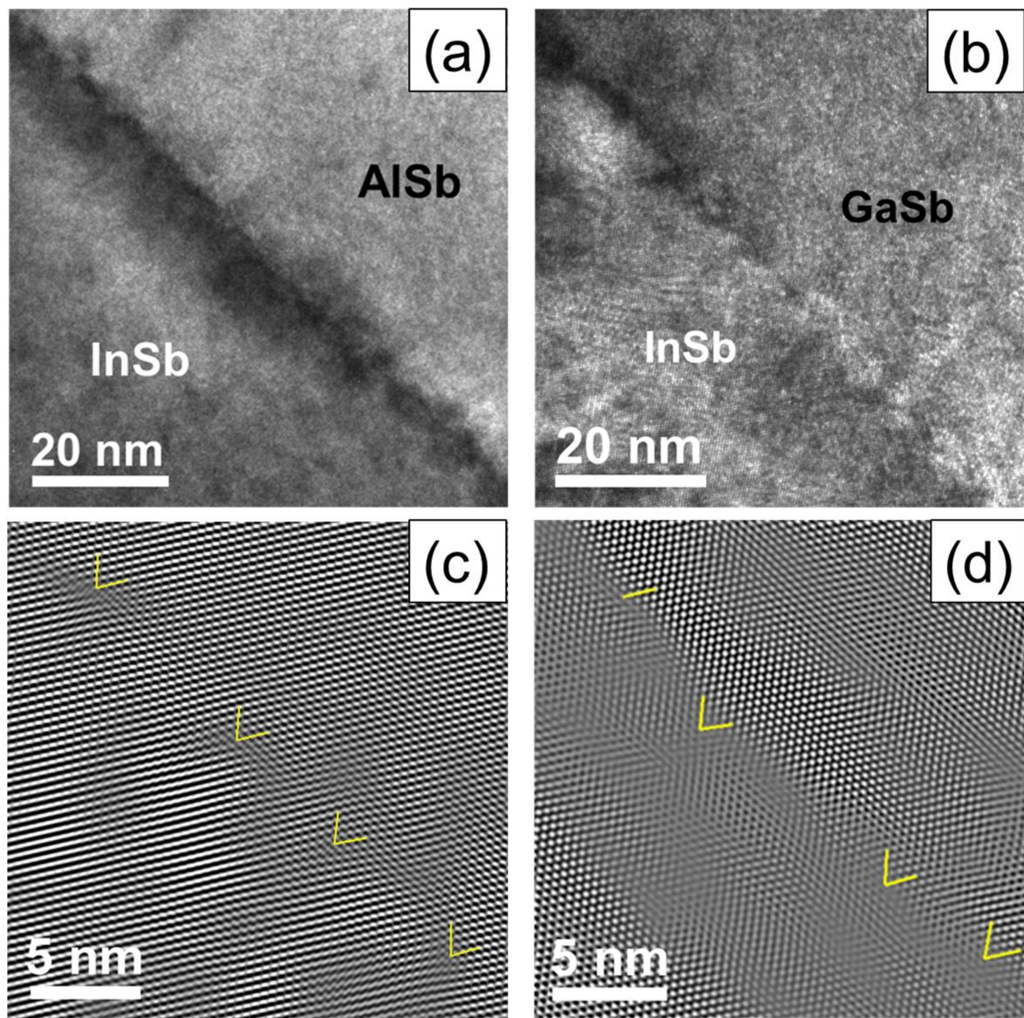

Fig. 6 Bright-field TEM images for (a) InSb/AlSb interface, (b) InSb/GaSb interface. (c) and (d) phase contrast images of (a) and (b), respectively by using Fourier mask filtering technique.

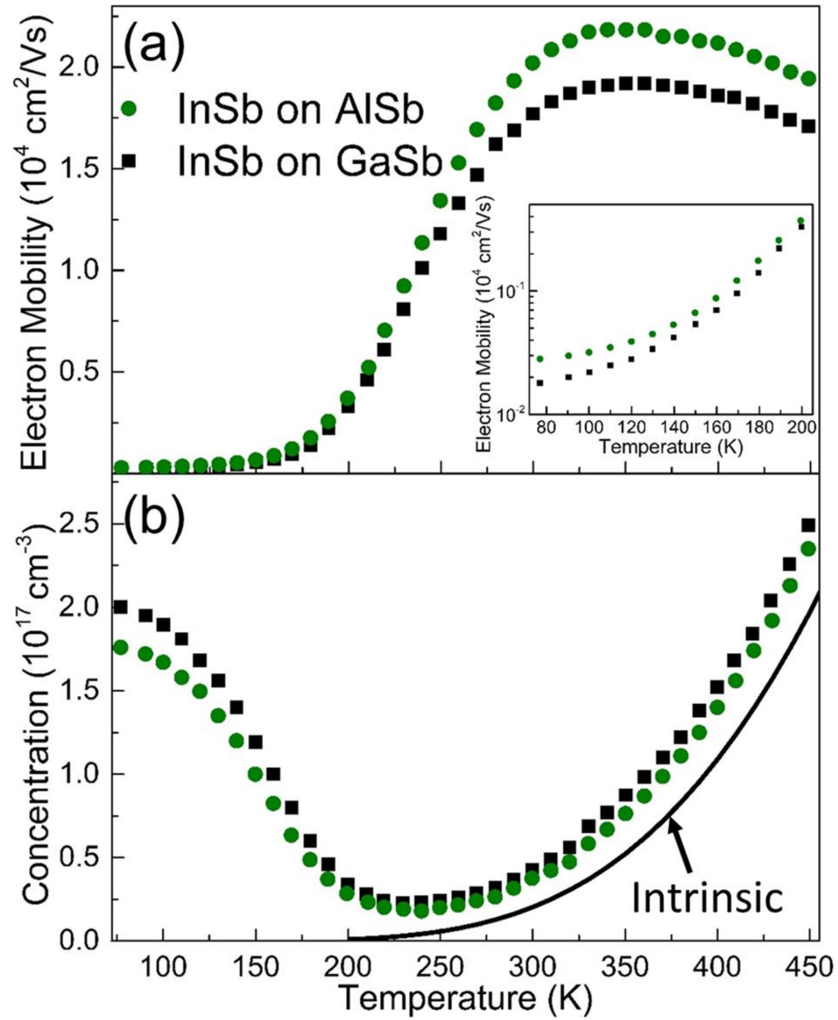

Fig. 7 Temperature dependence of (a) electron mobility and (b) concentration of InSb on Si with different buffer structures. The inset in (a) shows mobility from 80 K to 220 K. Intrinsic concentration was calculated using equation (2) and presented in (b).

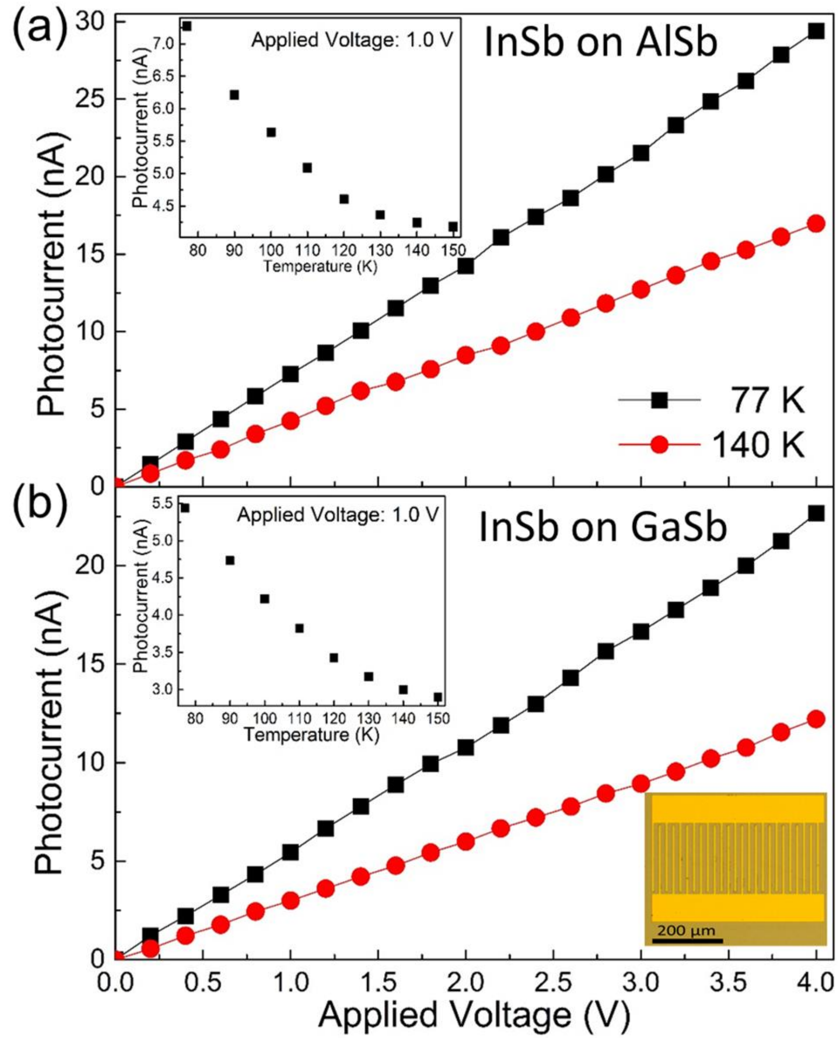

Fig. 8 Responsivity for (a) InSb photoconductor grown on AlSb and (b) InSb photoconductor grown on GaSb at 77 K and 140 K, respectively. Insets at the top left of (a) and (b) are the temperature dependent responsivity at 1.0 V from 77 K to 150 for InSb photoconductor grown on AlSb and GaSb, respectively. Inset at the bottom right of (b) is microscopic optical image of the InSb photoconductor.